Hindawi
International Journal of RF and Microwave Computer-Aided Engineering
Volume 2023, Article ID 3754725, 10 pages
https://doi.org/10.1155/2023/3754725

Research Article

A Theoretical Design of Angular-Phased Broadband Antenna Array for Submillimeter Wave Applications

Tushar Goel[1,2] **Anuradha Sonker,**[2] **A. K. Gautam**[3] **and Amalendu Patnaik**[2]

[1]Dept. of Electronics Engineering, National Institute of Technology Uttarakhand, Srinagar, Uttarakhand, India
[2]Dept. of Electronics & Communication Engineering, Indian Institute of Technology Roorkee, Uttarakhand, India
[3]Dept. of Electronics & Communication Engineering, G. B. Pant Institute of Engineering and Technology, Pauri, Uttarakhand, India

Correspondence should be addressed to A. K. Gautam; drakgautam@ieee.org

Received 16 February 2023; Revised 3 October 2023; Accepted 13 October 2023; Published 28 December 2023

Academic Editor: N. Nasimuddin

In this article, a broadband semicircular antenna array geometry was examined, along with its design and configuration in the submillimeter wave range (9.35-42.89 GHz). The work has been divided into two prime phases; in the first phase of work, an innovative angular-phased 1 : 4 broadband power divider has been presented in which its isolation, insertion, and return losses are investigated. In the next phase, the proposed power divider was used to configure a 4-element antenna array, and its theoretical analysis was carried out. The angular path difference in the array was used to introduce phase difference in between the antenna elements to minimize the mutual coupling and to optimize the narrow beamwidth. Using geometry and fundamental array theory, the array factor of a novel broadband array configuration has been derived and analytically investigated.

1. Introduction

Recently, much attention has been drawn to submillimeter-(mm-) wave antenna arrays for future radar, satellites, and wireless communication applications. The feeding network is always a crucial component in the design of radiating structure for an array configuration [1]. For this purpose, series or corporate feeding is frequently employed, and for corporate feeding, the feeding network requires power dividers. Various configurations of power dividers have been introduced to support planar circuit applications [2]. The design of a power divider is affected by important factors such as reflection coefficient, insertion loss, isolation, and bandwidth to measure the overall performance of significant communication systems. The most commonly used Wilkinson's power divider (WPD) is a great substitute for the designing of feed networks in antenna array systems due to its simple structure and minimum insertion loss [3–6]. However, WPD has drawbacks, such as narrow bandwidth and larger size due to the use of $\lambda/4$ transmission line sections at a single frequency.

To overcome these issues that are present in classical Wilkinson power splitter, several techniques have been suggested to increase the bandwidth of Wilkinson's power dividers using the methods such as open stubs [7], port extensions [8, 9], complementary conducting-strip transmission lines [10, 11], multisection techniques, and step impedance matching networks [12]. Rigorous analysis and investigation of the bandwidth broadening mechanism in the power divider with physical port isolation were also carried out to achieve the fractional bandwidth of 43.2% [13]. These techniques also report the use of lumped passive components instead of the transmission line section to reduce the circuit size and isolation loss between output ports. In an another approach, a wideband multisection Wilkinson power divider (WPD) circuit has been designed with the Euler method to calculate the characteristic impedance of WPD [14]. The percent bandwidth of the WPD was measured as 124.5% with minimum insertion loss. Another novel structure of the Wilkinson power divider with modified matching stub length has been discussed for the improvement in smaller size, low cost, equal power division,

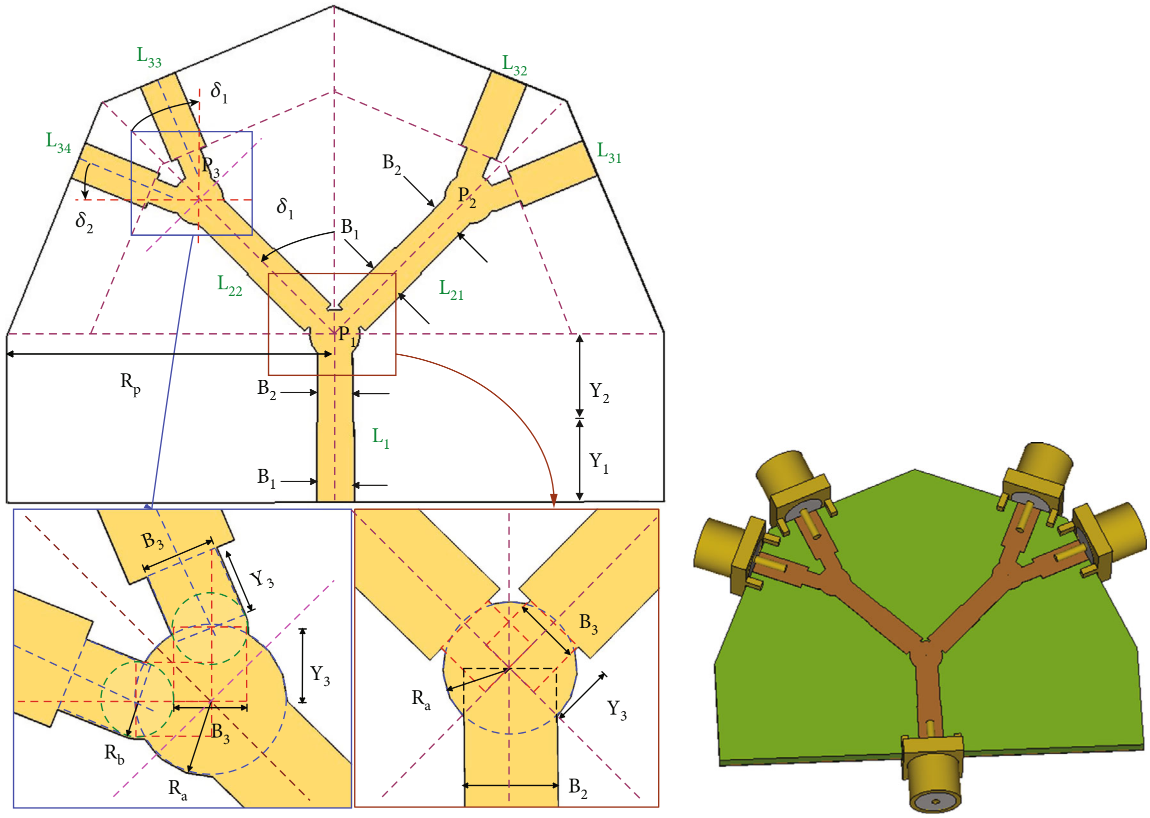

Figure 1: Wideband power divider configuration and its 3D front view.

minimum insertion loss, better isolation, and a satisfactory return loss of all ports incorporated into the antenna array feeding network [15].

An innovative concept was developed for the power splitter to use additional transmission lines between quarter wave transmission lines that improve physical and electrical isolation where the elements are placed between quarter wave transmission lines at an adjustable phase angle [16]. In order to meet the demanding standards of telecommunications technology, researchers have also made efforts to address the requirements of the broadband and multiband power dividers to achieve high data rates. These techniques include the dual-band Wilkinson power divider [11], compact power divider with narrow notch band [17], broadband Gysel power divider [18], miniature broadband four-way power divider [19], and compact wideband power divider [20, 21]. These broadband PDs improve return loss, isolation, and impedance matching at high frequencies. But such PDs become very complex and require a very large area to bend the output ports. Various analysis and design procedures on compact and simple wideband power dividers have been proposed in literatures [22–25]. A small, equal phase and equal power 1 : 4 wideband Wilkinson power divider was optimized in the range of 3.1 GHz-10.6 GHz [26]. A compact and easy wideband power divider was studied using linear tapered transmission lines in the frequency range of 3 GHz to 27 GHz to get the operational bandwidth of 24 GHz [27]. A conformal high-gain UWB 4-element array antenna with band rejection characteristics for WLAN applications was presented for the frequency from 3.6 to 12 GHz [28].

Table 1: Dimensions of the proposed power divider.

Parameter	Value	Parameter	Value
B_1	3 mm (0.261 λ)	Y_1	6.4 mm (0.56 λ)
B_2	2.8 mm (0.24 λ)	Y_2	7 mm (0.60 λ)
B_3	2 mm (0.174 λ)	Y_3	1.9 mm (0.165 λ)
R_a	2 mm (0.174 λ)	R_b	1 mm (0.087 λ)
δ_1	45°	δ_2	22.5°
Φ_0	30°	R_p	26.78 mm (2.33 λ)

In the context of the above discussion on power dividers, the classical WPD has a narrow bandwidth mainly due to two reasons: one is the abrupt discontinuity between the feeder and the radiator, and the other is the mutual coupling between the radiators [29]. In the proposed design, abrupt discontinuity is removed by using stepped microstrip line feeding, and the junctions are made circular to overcome the losses due to mismatching. As a result, current travels longer path which causes an increase in electrical length. On the other hand, mutual coupling among the radiators are minimized by optimizing the angular distance among the receiver ports. By this novel configuration, a proposed design is able to get a good trade-off between strong isolation and high operational bandwidth in the design of power divider for wideband antenna array in sub-mm wave range. The work is divided into two prime phases: phase-I consists

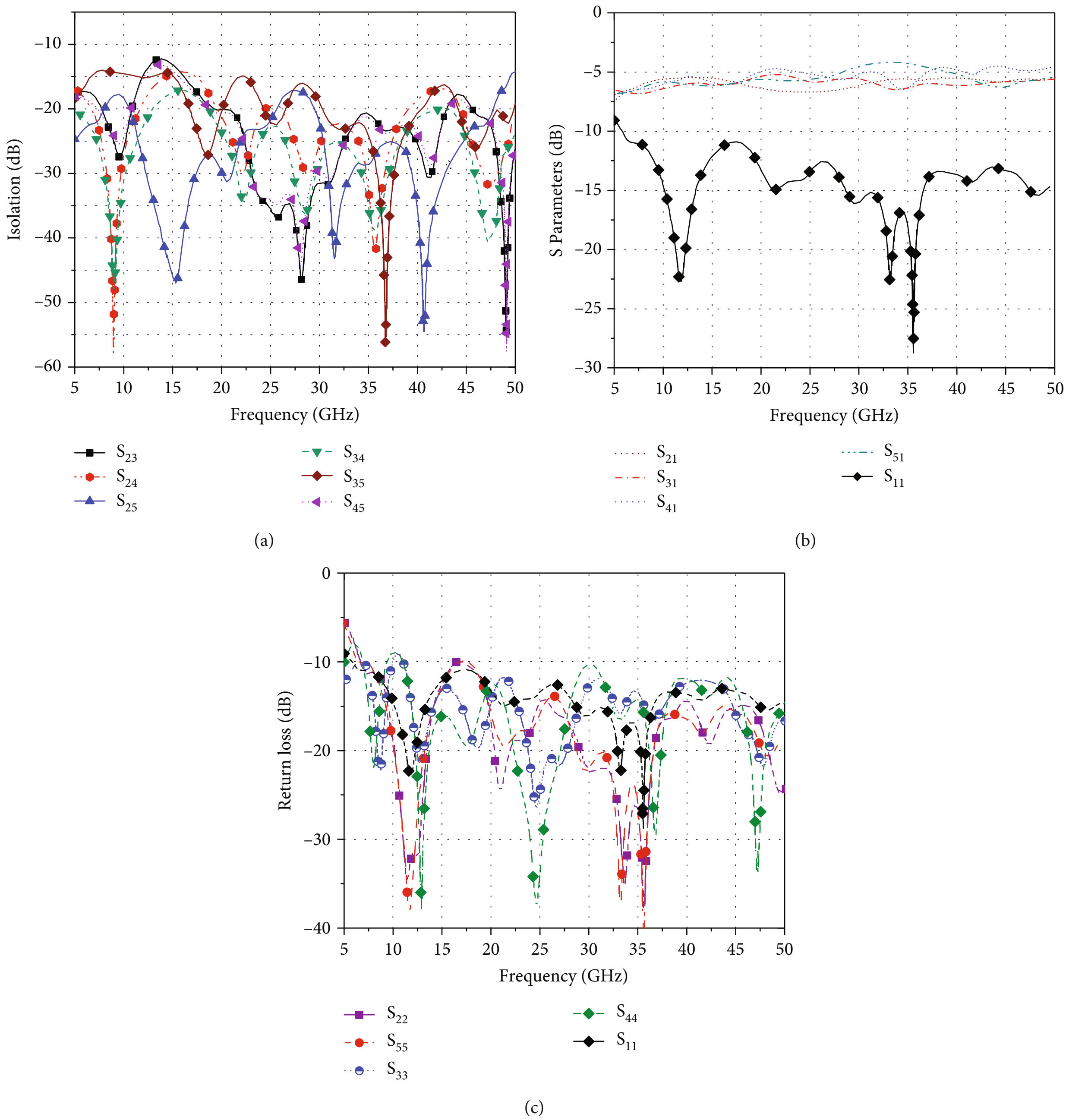

Figure 2: Simulated (a) isolation (dB), (b) insertion loss (dB), and (c) return loss vs. frequency curves.

of an innovative angular-phased 1 : 4 broadband power divider in which its isolation, insertion, and return losses are investigated. In phase-II, the proposed power divider is used to design an antenna array, and its theoretical analysis is carried out.

The Wilkinson power divider is frequently used in traditional linear arrays to distribute power across the array elements that are linearly arranged. Nonlinear phased arrays had been used in certain previously documented approaches to steer the radiating beam of many antenna elements in a specific direction. Using bow-tie radiators, a 4-element subarray with a central feeding was created in [30] in which subarray was considered as a single element; then, there were 32 elements total scattered around the surface of the octal prism, which had 4 subarrays on each of its four sides. In order to determine the direction of arrival, six sides and the top of the truncated hexagonal pyramid were dispersed with seven coaxially fed microstrip patch antennas [31]. To create the directional array antennas, a few various feeding approaches, including closely linked multifeed, SIW series-parallel differential feeding network, and centrally fed by substrate integrated coaxial line, were presented [32–40].

Even though numerous types of array structures have been discussed in recent years, broadband array antennas in the sub-mm wave region, which are highly desired in particular for future mobile technologies and short-range communication applications, have not yet been extensively examined. The suggested array's innovative design offers angular path difference rather than linear path difference, as in other traditional arrays, increasing the structure's compactness and enabling effective impedance matching across a broad frequency range in sub-mm wave. In the following subsections, the proposed antenna array is explored extensively from the perspective of antenna design, configuration, and various result curves.

2. Configuration of Power Divider

In the proposed configuration, abrupt discontinuity is removed by increasing the electrical length of the feeding by utilizing stepped microstrip line feeding to overcome the losses due to mismatch as shown in Figure 1. The dimensions of the proposed power divider are mentioned in Table 1, and the electrical length of these parameters is calculated at a center frequency of 26.12 GHz. Each subsection of the main feedline is having a size of $B_1 \times Y_1$ and $B_2 \times Y_2$, respectively. These two subsections together were considered as the main microstrip line L_1 for the excitation. Two similar branches having the width of B_3 and length of Y_3 were extracted out from the primary microstrip line L_1 at an angle of δ_1, either side from its axis for the power distribution. By rotating these sublines, angular path difference was created among the subbranches. As a result, mutual coupling among these subbranches can be minimized by optimizing the angular distance among the receiver ports.

These feed lines were further extended by microstrip line L_1 and were considered as the feed lines L_{21} and L_{22}. For current smoothening, a circle of radius of R_a was drawn, considering the rotation point of the branches as the center of the circle. It was the first junction P_1, from which the power was distributed from L_1 to L_{21} and L_{22}. The circle at the junction P_1 smoothens the flow of current, and in another way, it allows the travelling wave to overcome the losses so far and to retrieve its strength.

Similarly, other junctions were formed by extracting out the two more branches with the width of B_3 and the length of Y_3 from the L_{21} and L_{22} at an angle of δ_1, either side from the axis of the lines, for the power distribution. Again the circle of radius of R_a was drawn at the junction point for current smoothening. All the four extracted branches were further extended with the dimensions same as L_{21} and L_{22} but rotated at an angle of δ_1 from the horizontal axis. To remove the discontinuity and for current smoothening, again, circles having the radius of R_a were drawn as shown in the green (left) inset in Figure 1. Thus, two more junctions (P_2 and P_3) were created to distribute the power from L_{21} to L_{31} and L_{32} and from L_{22} to L_{33} and L_{34}.

Considering the port of the main branch as port 1 and ports of four subbranches S in a counter-clockwise direction as port 2-port 5, respectively, parameters of all the ports were calculated by using a 2.92 mm connector at each port for considering the losses due to connectors under the real-time practical conditions in the CST MWS simulator.

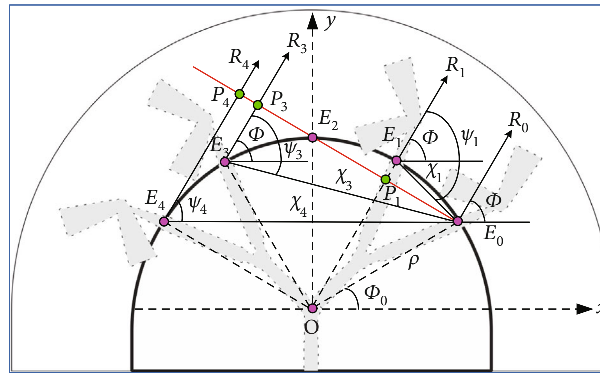

Figure 3: Geometry of semicircular antenna array.

Figure 2(a) shows the isolation among the ports, and it is to be noticed from the said figure that isolation curves for S_{23}, S_{35}, and S_{45} are below -13 dB, whereas it is far below -16 dB for S_{24}, S_{25}, and S_{34} throughout the frequency range. Insertion and reflection coefficient curves for input port 1 are shown in Figure 2(b), in which plots of S_{11}, S_{21}, S_{31}, S_{41}, and S_{51} are shown. As expected, reflection coefficient S_{11} is far below -10 dB, and insertion from port 1, representing the S-parameters S_{21}, S_{31}, S_{41}, and S_{51}, has approximated range of -6 dB to -4 dB in the entire range. Self-reflection at the other ports is presented in Figure 2(c), and as observed, reflection coefficients at ports 2, 3, 4, and 5 are meeting the expectations of being below -10 dB in the entire frequency range. It can also be analyzed in Figure 1 that there is a grouping of ports 2 and 3 and ports 4 and 5 together; in the same fashion, their return loss curves shown in Figure 2(c) are also matched throughout the operating range. It can be concluded that this novel configuration of a proposed power divider is able to attain a good trade-off between strong isolation and high operational bandwidth in sub-mm wave range. Once the power divider is ready, it can now be utilized for configuring the broadband antenna array which is discussed in the subsequent section.

3. Analysis and Design of the Array

At present, researchers and communication scientists are collaborating on design of beam-forming broadband networks using massive MIMO antenna systems for future short-range communication pursposes in sub-mm wave range. For this purspose, highly directive antenna arrays are required to be embedded in massive MIMO system so that multibeam forming networks may be implemented. Aiming this, a semicircular array (SCA) was implemented, using the proposed power divider for 50 Ω input impedance feedline in which a single antenna element was used that is a broadband (10-150 GHz) antipodal end-fire antenna, proposed by the authors recently [41]. To further improve the gain and directivity of the single element, this antenna was configured in an array configuration, as can be seen in Figure 3, which depicts the top perspective of the proposed array structure. According to Figure 1, four single element antennas were placed at the center points of the terminating

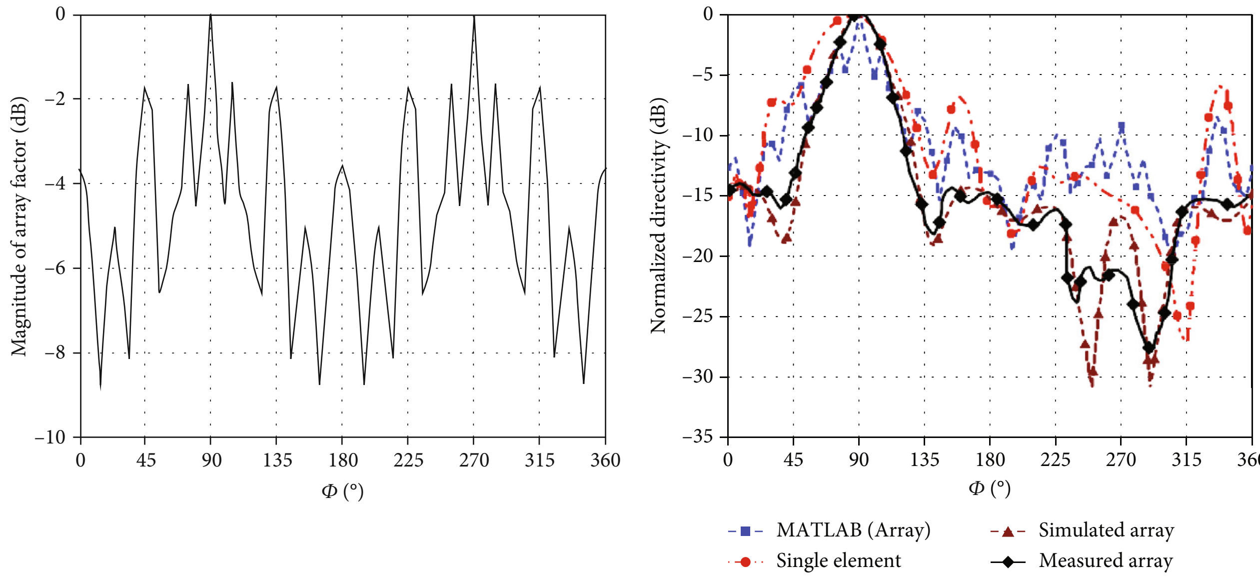

(a) (b)

Figure 4: (a) Magnitude of array factor vs angle phi (degree) isolation (dB) at 21.6 GHz and (b) comparison of normalized radiation pattern curves of the single element antenna vs. semicircular array at 21.6 GHz.

edges of lines L_{31}, L_{32}, L_{33}, and L_{34}, respectively. When calculating the values of δ_1 and δ_2, as shown in Figure 1 by the dotted line, it was considered that all four antenna elements were positioned orthogonally at the outermost edges of the semi-four octagon. The initial power junction node, P1, is located in the center of the semioctagon. These feed lines were rotated at an angle of δ_1 from either side of their axes in order to produce the appropriate angular path difference between antenna elements to achieve desired highly directional power pattern and operational range. This is due to the fact that it has a direct impact on the antenna components' mutual coupling.

Since each branch of an octagon makes an internal angle of 45° from the origin according to geometry, $\delta_1 = 45^\circ$ and $\delta_2 = 22.5^\circ$, an antenna element might be placed at an angle of 90° from the edge of the semioctagon. Consequently, the angular phase shift between the antenna components is $\lambda/4$. This whole array configuration was created on a semicircular Rogers RO4232 substrate with a thickness of 1.52 mm and a radius of R_{sub}. The geometry of the semicircular array (SCA) is presented in Figure 3, and it can be observed that point O is the center of the semicircle of radius $\rho = 37$ mm which lies in the x-y plane. This semicircle was divided into six sections, and each section has an arc angle of Φ_0 with respect to the center of the semicircle. The derivation of array factor of semicircular array was carried out with the following assumptions [42]:

(1) Single element antennas of the array were treated as the individual point sources, located at the center of their respective radiation patterns (points E_0, E_1, E_3, and E_4)

(2) Current supplied to each antenna element was of same magnitude and phase

(3) There was no mutual coupling among the antenna elements

(4) The radiation pattern of the antenna array was observed in the far field, and hence, field vectors from all sources $\mathbf{R_1}$, $\mathbf{R_3}$, and $\mathbf{R_4}$ were parallel to each other and were at an arbitrary angle of Φ from the x-axis

The element E_0 was assumed as the reference point for the semicircular array. Angles between line segments $\overline{E_1E_0}$, $\overline{E_3E_0}$, $\overline{E_4E_0}$ and field vectors $\mathbf{R_1}$, $\mathbf{R_3}$, and R_4 are Ψ_1, Ψ_3, Ψ_4, respectively. Using geometry, angles Ψi were calculated in degree and can be expressed as

$$\Psi_i = 90^\circ + \Phi - \left(\frac{i}{2} + 1\right)\Phi_0, \tag{1}$$

where $i = 1, 3, 4$ and Φ is the angle made by the antenna field vectors $\mathbf{R_1}$, $\mathbf{R_3}$, and $\mathbf{R_4}$ from the x-axis.

The line segments from the reference element E_0 to the antenna elements E_1, E_3, and E_4, are χ_1, χ_3, and χ_4, respectively. The χ i was calculated by geometry, in terms of radius ρ and angle Φ_0 and can be expressed as

$$\chi_i = 2\rho \mathrm{Sin}\left(\frac{i\Phi_0}{2}\right), \tag{2}$$

where $i = 1, 3, 4$. The path differences were calculated from the angles Ψ_1, Ψ_3, and Ψ_4 and line segments χ_1, χ_3, and χ_4 as shown in Figure 3. The relative path differences from the E_0 for the antenna elements E_1, E_3, and E_4 are the line segments $\overline{E_1P_1}$, $\overline{E_3P_3}$, and $\overline{E_4P_4}$ which are notated as α_1, α_3,

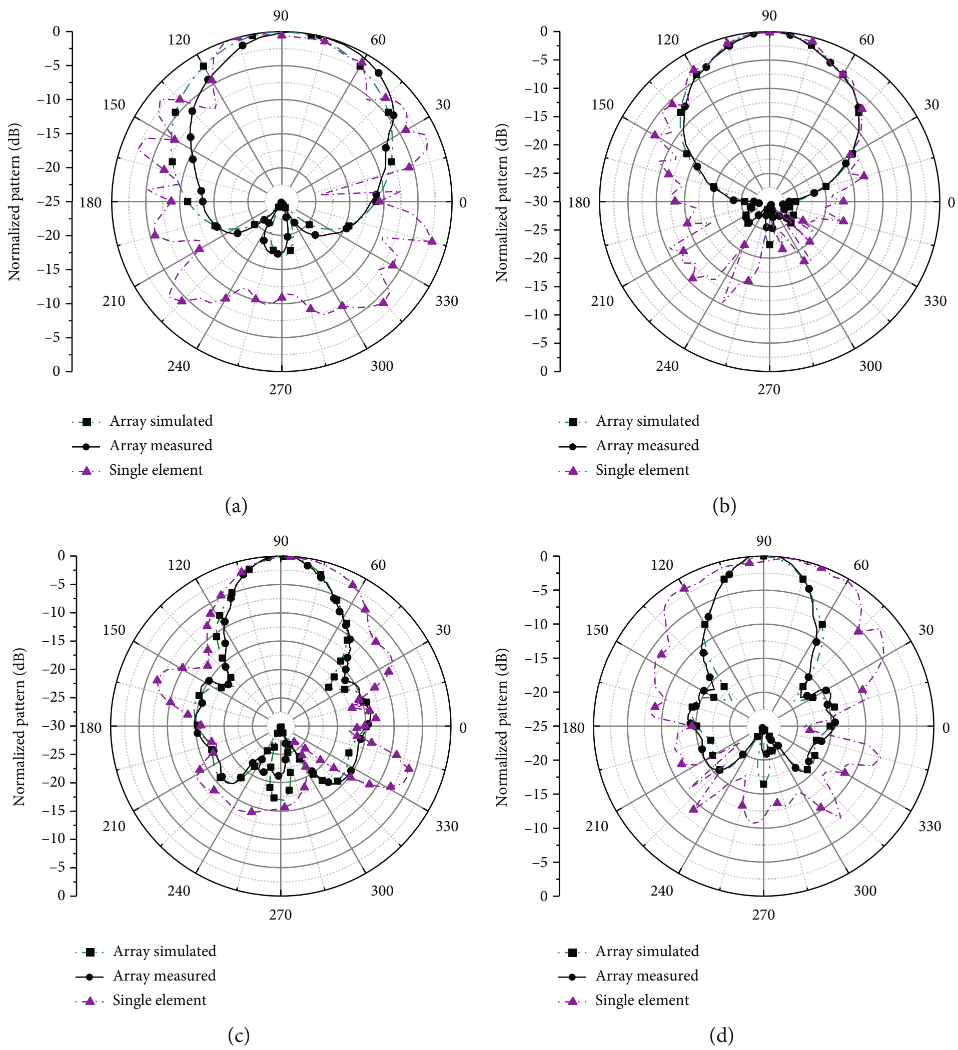

Figure 5: Comparison of 2D power pattern in $\phi = 90^\circ$ plane of proposed array vs. single element at intermediate frequencies in GHz: (a) 11, (b) 18, (c) 26, and (d) 36.

and α_4, respectively, and can be expressed as

$$\alpha_i = \chi_i \mathrm{Cos}(\Psi_i), \tag{3}$$

where $i = 1, 3, 4$. By array theory, array factor of the semicircular array can be computed as

$$\mathrm{AF} = 1 + \sum_{i=1}^{4} e^{\mathrm{jk}\alpha_i}, \tag{4}$$

where $i \neq 2$ and k is the phase constant. By putting the values of Ψ_i, χ_i, and α_i from eqs. (1)–(3), respectively, eq. (4) can be rewritten as

$$\mathrm{AF} = 1 + \sum_{i=1}^{4} e^{-j2k\rho \mathrm{Sin}(a_{1i})\mathrm{Sin}(\Phi - b_{1i})}, \tag{5}$$

where $a_{1i} = [15^\circ \quad 0 \quad 45^\circ \quad 60^\circ]$, $b_{1i} = [45^\circ \quad 0 \quad 75^\circ \quad 90^\circ]$, and $i \neq 2$

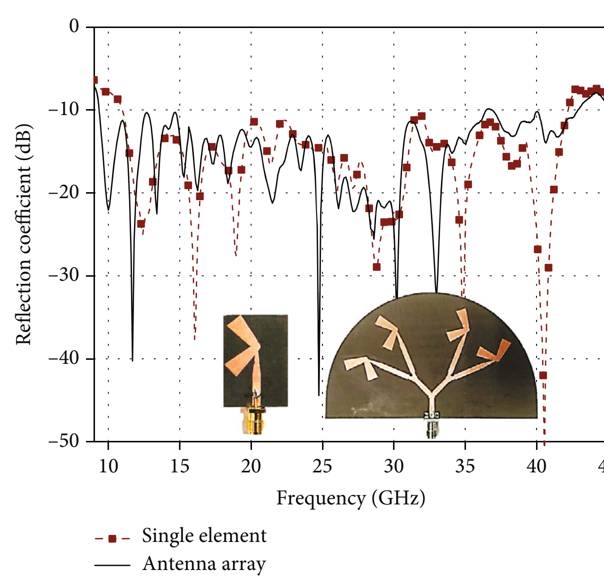

Figure 6: Comparison of experimental reflection coefficient of the Single element antenna Vs proposed antenna array.

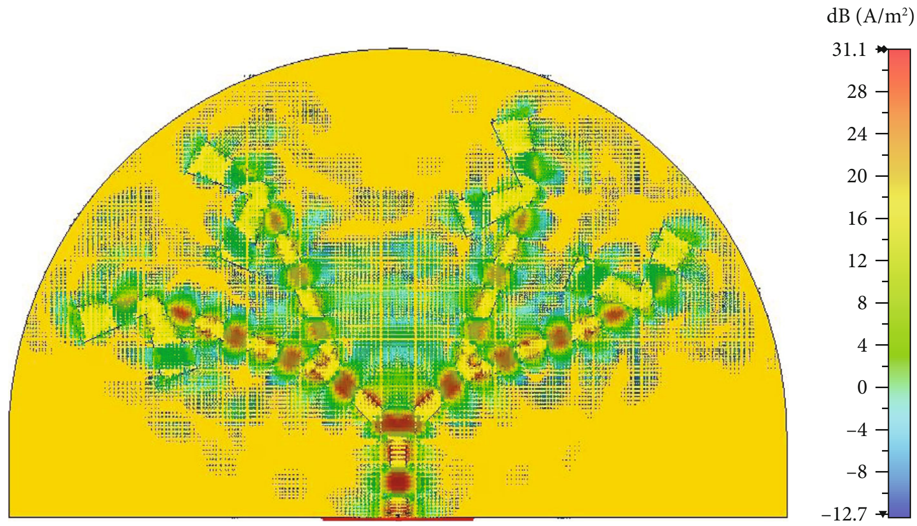

Figure 7: Current density distribution of proposed array at 21.6 GHz.

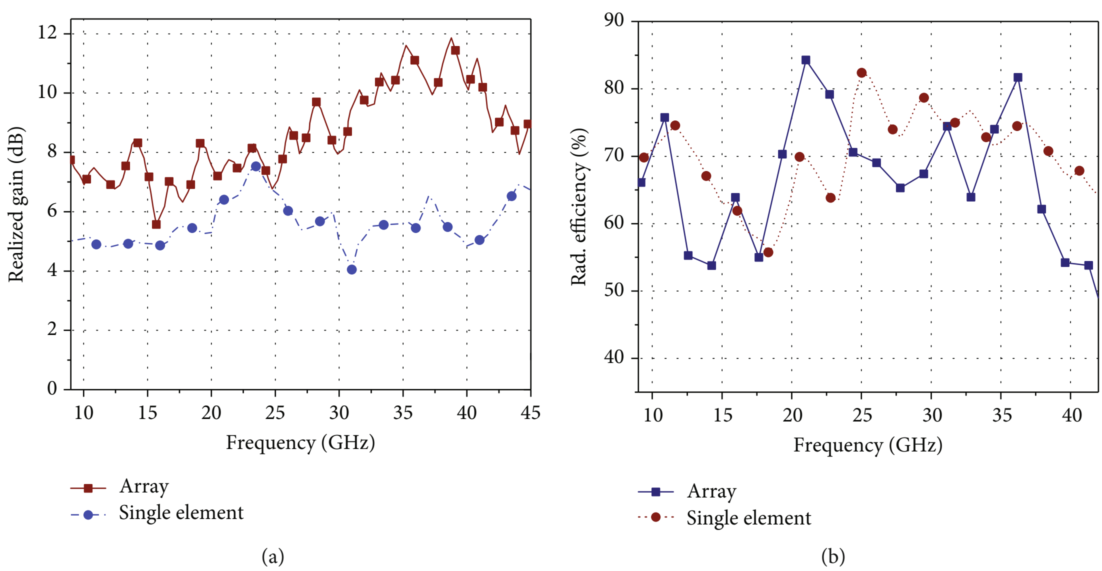

Figure 8: Comparison between proposed array vs. single element (a) realized gain (dB) and (b) radiation efficiency (%).

The magnitude of array factor was derived from eq. (5) and can be expressed as

$$|\mathrm{AF}| = \sqrt{\left(4 + 2\sum_{n=1}^{6} \mathrm{Cos}\left(\frac{2 \times 180 \times k \times \rho \times \zeta_n}{\pi}\right)\right)}, \quad (6)$$

where $\zeta_n = \mathrm{Sin}(a_{1n}) \times \mathrm{Sin}(b_{1n} - \Phi)$.

$$\begin{aligned} a_{1n} &= [15^\circ \quad 45^\circ \quad 60^\circ \quad 30^\circ \quad 45^\circ \quad 15^\circ], \\ b_{1n} &= [45^\circ \quad 75^\circ \quad 90^\circ \quad 90^\circ \quad 105 \quad 135^\circ]. \end{aligned} \quad (7)$$

To determine the point of maxima in eq. (6), the magnitude of array factor at centre center frequency 21.6 GHz, with respect to the angle phi (degree) was plotted as shown in Figure 4(a). It can be observed that magnitude of array factor is maximum at $\Phi = 90^\circ$ and $\Phi = 270^\circ$ proving that the direction of the main lobe of SCA is $\Phi = 90^\circ$ and $\Phi = 270^\circ$ which could have been the same in the linear phased array. As a result, the semicircular array obtained the same relative path difference among antenna components as the linear phased array. The main difference between linear and proposed phased array is the calculation of path difference. The required path difference among the antenna elements is achieved by linear displacement in the linear phased array and by angular displacement in the proposed semicircular phased array. The main advantages of the proposed array arrangement over the conventional array is size reduction, which is a crucial factor for space-borne antennas; minimal mutual coupling, and broadband characteristics.

Normalized directivity plot of a single antenna element predicted by CST MWS and a 4-element semicircular

Table 2: Comparison of the proposed word with other relevant state-of-the-art designs.

Ref.	No. of radiating elements	Frequency range	Gain (dB)	Fractional bandwidth
[44]	8	55-66 GHz	9-12	18.18%
[45]	64	18.7-33.15 GHz	18-21	55.7%
[46]	4	26.5-36 GHz	15-17	30.4%
[47]	22	1.19-11.7 GHz	4-7.5	163%
[48]	4	28-40 GHz	5-8	35.29%
[49]	6	6-18 GHz	Not Provided	100%
[50]	4	3-13.2 GHz	2-4	125.9%
[51]	16	15.4-46.4 GHz	10-16	100.32%
[52]	4	24.4-29.5 GHz	Negative	18.92%
[53]	8	27.4-28.6 GHz	2.5-4	4.2%
[54]	4	22-31 GHz	4-8	33.96%
[55]	16	7-21 GHz	0-5	100%
[56]	4	4-18 GHz	Negative	127.27%
This Work	4	9.35-42.89 GHz	5.22-11.86	128.4%

antenna array, calculated on MATLAB using pattern multiplication principle [42], at 21.6 GHz is shown in Figure 4(b). Particular reason of choosing 21.6 GHz was that it is the only resonant frequency of the SCA which is not only closest to the center frequency of the band (10 GHz to 42 GHz) but also nearest to the resonance frequency (22.5 GHz) of the single element antenna at which normalized directivity plot in H-plane was analyzed in [41]. It can be observed in Figure 4(b) that by modifying the single-element antenna into SCA, the direction of the maximum radiation remains the same for both the antenna and the array that is $\Phi = 90^{\circ}$, while the gain was significantly improved and array becomes highly direction as 3 dB angular beamwidth was decreased to 32° from 65.5°. There was tremendous change in the sidelobe level as well those were reduced to -14.1 dB from -0.5 dB for the earlier case. The same has been reflected in Figure 5 in which updations in polar patterns for $\phi = 90^{\circ}$ from single element to array is analyzed. Thus, it can be concluded that radiation properties of the antenna array got highly improved compared to single element antenna, from the perspective of the gain as well as the directivity.

Measured reflection coefficient comparison between the single antenna element and proposed SCA is represented in Figure 6 along with the lab-fabricated prototypes, and it ensures the -10 dB impedance matching in both cases. According to the said figure, both single-element and antenna arrays comprise wide impedance bandwidth in the sub-mm wave range. The current density distribution of the proposed array at 21.6 GHz is shown in Figure 7; from the rainbow scale, it is analyzed that power is equally distributed among the antenna elements, and the mutual coupling among the antenna elements is all blue that shows minimal coupling, that results to broadband operation. The junctions are all red that shows the perfect distribution of the power at the circular junction. Figure 8(a) comprises the improvement of realized gain from the single-element to the 4-element antenna array. From the said figure, it is concluded that the average gain in array conversion goes up from 6.42 dB to 8.55 dB in sub-mm wave range 9 to 45 GHz. The effect in radiation efficiency is shown in Figure 8(b), which concludes that in both cases, average radiation efficiency is approximately 69.17%, which is fine at such a high range, meaning both the structures are radiating well in this range. Thus, from all discussed result analysis, it can be concluded that the radiation properties of the antenna array got highly improved compared to single element antenna, from the perspective of the gain as well as the directivity.

The performance of the proposed work is compared to that of other analogous low-profile and broadband end-fire antenna arrays in Table 2. As far as any of us are aware, the proposed SCA performs far better than any other known array structure in the suggested operating frequency range in terms of impedance bandwidth and gain.

4. Conclusion

An overview of the proposed semicircular antenna array architecture, as well as its design and configuration, was accomplished both theoretically and empirically. The designed antenna array was arranged with an angular phased 1 : 4 power divider, in which abrupt discontinuity was avoided using stepped microstrip line feeding, and the circular junctions were provided to prevent mismatching losses. Due to the increment of electrical length, current takes longer path to travel that causes compactness in the design as it allowed the antenna to radiate at lower frequencies as well. On the other hand, the sublines' rotation created an angular path difference in between its subbranches. As a result, by optimizing the angular distance between the receiver ports, mutual coupling among the radiators in the array feed by these subbranches was minimized that allows wideband operation of the array. The array factor of a novel array arrangement was computed using geometry and fundamental array theory, and it has been mathematically shown that for the proposed structure, the direction of maximum radiation is $\Phi = 90^{\circ}$ that is the end-fire H-plane. While comparing normalized directivity plots of the proposed 4-element array configuration to the single element, it was found that the antenna gain, directivity, angular beamwidth, and side lobe levels were all much improved when utilising the proposed array design. It can be concluded that in the sub-mm wave region, the proposed power divider's innovative structure achieves a favourable trade-off between robust isolation and large operating bandwidth. The aforementioned array can be used in the design of multibeamforming massive MIMO systems for long- and short-range communication networks in the future [43].

Data Availability

Raw data were generated at the research lab of the National Institute of Technology, Uttarakhand. Derived data supporting the findings of this study are available from the corresponding author, Dr. A. K Gautam, on request.

Conflicts of Interest

No potential competing interest was reported by the authors.

References

[1] K. C. Gupta, K. C. Gupta, and M. D. Abouzahra, *Analysis and Design of Planar Microwave Components*, IEEE Press, 1994.

[2] D. M. Pozar, *Microwave Engineering Theory and Techniques: An Indian Adaptation*, John wiley & Sons, 2020.

[3] E. J. Wilkinson, "An N-way hybrid power divider," *IRE Transactions on Microwave Theory and Techniques*, vol. 8, no. 1, pp. 116–118, 1960.

[4] L. Parad and R. Moynihan, "Split-tee power divider," *IEEE Transactions on Microwave Theory and Techniques*, vol. 13, no. 1, pp. 91–95, 1965.

[5] S. B. Cohn, "A class of broadband three-port TEM-mode hybrids," *IEEE Transactions on Microwave Theory and Techniques*, vol. 16, no. 2, pp. 110–116, 1968.

[6] R. B. Ekinge, "A new method of synthesizing matched broadband TEM-mode three-ports," *IEEE Transactions on Microwave Theory and Techniques*, vol. 19, no. 1, pp. 81–88, 1971.

[7] A. Sanadhya, A. Mathur, M. S. Chouhan, and K. Singh, "Design of Wilkinson power divider using stubs," in *18-th International Conference on Microwaves, Radar and Wireless Communications*, pp. 1–4, Vilnius, Lithuania, 2010.

[8] M. J. Park, "Dual-band Wilkinson divider with coupled output port extensions," *IEEE Transactions on Microwave Theory and Techniques*, vol. 57, no. 9, pp. 2232–2237, 2009.

[9] M. Park and B. Lee, "Wilkinson power divider with extended ports for dual-band operation," *Electronics Letters*, vol. 44, no. 15, p. 916, 2008.

[10] Z. Li, L. Lv, R. Zeng, and J. Lv, "A compact wideband Wilkinson power divider using periodic synthesized transmission line in silicon IPD process," in *2019 49th European Microwave Conference (EuMC)*, pp. 133–136, Paris, France, 2019.

[11] X. Wang, I. Sakagami, K. Takahashi, and S. Okamura, "A generalized dual-band Wilkinson power divider with parallel L, *C*, and *R* components," *IEEE Transactions on Microwave Theory and Techniques*, vol. 60, no. 4, pp. 952–964, 2012.

[12] T. Yu and J. H. Tsai, "Design of multiway power dividers including all connecting lines," *IET Microwaves, Antennas & Propagation*, vol. 12, no. 8, pp. 1367–1374, 2018.

[13] A. Desai, Y. F. Tsao, T. J. Chang et al., "Rigorous analysis and investigation of the bandwidth broadening mechanism in a compact power divider with physical port isolation," *IEEE Access*, vol. 10, pp. 133655–133662, 2022.

[14] Ö. Kasar and M. Kahriman, "A theoretical design of ultra-wideband multisection Wilkinson power divider using Euler polynomials," *Microwave and Optical Technology Letters*, vol. 62, no. 12, pp. 3869–3875, 2020.

[15] F. A. Shaikh, S. Khan, A. Z. Alam, M. H. Habaebi, O. O. Khalifa, and T. A. Khan, "Design and analysis of 1-to-4 Wilkinson power divider for antenna array feeding network," in *2018 IEEE International Conference on Innovative Research and Development (ICIRD)*, pp. 1–4, Bangkok, Thailand, 2018.

[16] X. Wang, I. Sakagami, A. Mase, and M. Ichimura, "Trantanella Wilkinson power divider with additional transmission lines for simple layout," *IET Microwaves, Antennas & Propagation*, vol. 8, no. 9, pp. 666–672, 2014.

[17] F. Wei, W. T. Li, X. W. Shi, and Y. Y. Wang, "Design of compact inphase power divider with one narrow notch band for UWB application," *Electronics Letters*, vol. 48, no. 3, pp. 166–168, 2012.

[18] F. Lin, Q. X. Chu, Z. Gong, and Z. Lin, "Compact broadband Gysel power divider with arbitrary power-dividing ratio using microstrip/slotline phase inverter," *IEEE Transactions on Microwave Theory and Techniques*, vol. 60, no. 5, pp. 1226–1234, 2012.

[19] T.-H. Tseng and Y.-S. Lin, "Miniature broadband four-way power divider in glass-based thin-film integrated passive device technology," in *2013 IEEE MTT-S International Microwave Symposium Digest (MTT)*, pp. 1–4, Seattle, WA, USA, 2013.

[20] Y. S. Lin and J. H. Lee, "Miniature ultra-wideband power divider using bridged T-coils," *IEEE Microwave and Wireless Components Letters*, vol. 22, no. 8, pp. 391–393, 2012.

[21] W. Choe and J. Jeong, "Compact modified Wilkinson power divider with physical output port isolation," *IEEE Microwave and Wireless Components Letters*, vol. 24, no. 12, pp. 845–847, 2014.

[22] M. Weng, Y. Song, and J. Zhao, "Design of compact microstrip UWB power divider using square ring multiple-mode resonator," in *2015 Asia-Pacific Microwave Conference (APMC)*, pp. 1–3, Nanjing, China, 2015.

[23] Z. Yang, B. Luo, J. Dong, and T. Yang, "Ultra-wideband power divider employing coupled line and short-ended stub," *Microwave and Optical Technology Letters*, vol. 58, no. 3, pp. 713–715, 2016.

[24] S. A. M. Osman, A. M. E. El-Tager, F. I. Abdelghany, and I. M. Hafez, "Two-way modified Wilkinson power divider for UWB applications using two sections of unequal electrical lengths," *Progress In Electromagnetics Research C*, vol. 68, pp. 221–233, 2016.

[25] A. El Alami, S. Das, B. Madhav, and S. D. Bennani, "Design, optimization and realization of high gain RFID array antenna 4×1 for detection system of objects in motion," *Journal of Instrumentation*, vol. 14, no. 5, article P05002, 2019.

[26] A. H. Ali, R. A. Abd-Alhameed, J. M. Noras, and M. B. Child, "An ultra wide band power divider for antenna array feeding network," in *2016 Loughborough Antennas & Propagation Conference (LAPC)*, pp. 1–4, Loughborough, UK, 2016.

[27] F. Razzaz, S. M. Saeed, and M. A. S. Alkanhal, "Compact ultra-wideband Wilkinson power dividers using linearly tapered transmission lines," *Electronics*, vol. 11, no. 19, p. 3080, 2022.

[28] S. Lakrit, H. Medkour, S. Das, B. T. P. Madhav, W. A. Ali, and R. Dwivedi, "Design and analysis of integrated Wilkinson power divider- fed conformal high-gain UWB array antenna with band rejection characteristics for WLAN applications," *Journal of Circuits, Systems and Computers*, vol. 30, no. 8, article 2150133, 2021.

[29] Y. Liu, S. Sun, and L. Zhu, "2^n-way wideband filtering power dividers with good isolation enhanced by a modified isolation network," *IEEE Transactions on Microwave Theory and Techniques*, vol. 70, no. 6, pp. 3177–3187, 2022.

[30] K. R. Mahmoud and A. M. Montaser, "Performance of tri-band multi-polarized array antenna for 5G mobile base station adopting polarization and directivity control," *IEEE Access*, vol. 6, pp. 8682–8694, 2018.

[31] S. Mohammadi, A. Ghani, and S. H. Sedighy, "Direction-of-arrival estimation in conformal microstrip patch array antenna," *IEEE Transactions on Antennas and Propagation*, vol. 66, no. 1, pp. 511–515, 2018.

[32] K. Wu, Y. Yao, X. Cheng, T. Xiu, J. Yu, and X. Chen, "Wideband circularly polarized septum antenna array with ridge gap waveguide feeding network for wireless application," *IEEE Transactions on Antennas and Propagation*, vol. 70, no. 5, pp. 3882–3887, 2022.

[33] S. Islam, M. Zada, and H. Yoo, "Highly compact integrated Sub-6 GHz and millimeter-wave band antenna array for 5G smartphone communications," *IEEE Transactions on Antennas and Propagation*, vol. 70, no. 12, pp. 11629–11638, 2022.

[34] D.-F. Guan, Z.-P. Qian, Y.-S. Zhang, and J. Jin, "High-gain SIW cavity-backed array antenna with wideband and low sidelobe characteristics," *IEEE Antennas and Wireless Propagation Letters*, vol. 14, pp. 1774–1777, 2015.

[35] C. X. Mao, M. Khalily, P. Xiao, T. W. C. Brown, and S. Gao, "Planar sub-millimeter-wave array antenna with enhanced gain and reduced sidelobes for 5G broadcast applications," *IEEE Transactions on Antennas and Propagation*, vol. 67, no. 1, pp. 160–168, 2019.

[36] Q. Liang, H. Aliakbari, and B. K. Lau, "Co-designed millimeter-wave and sub-6 GHz antenna for 5G smartphones," *IEEE Antennas and Wireless Propagation Letters*, vol. 21, no. 10, pp. 1995–1999, 2022.

[37] L. Cheng, K. K. Fan, Z. C. Hao, and W. Hong, "Compact and wideband millimetre wave circularly polarised antenna array based on a SICL to waveguide transition," *IET Microwaves, Antennas & Propagation*, vol. 11, no. 14, pp. 2097–2103, 2017.

[38] S. Komeylian, "Deep neural network modeling of different antenna arrays; analysis, evaluation, and application," *IEEE Canadian Journal of Electrical and Computer Engineering*, vol. 44, no. 3, pp. 261–274, 2021.

[39] A. Farahbakhsh, D. Zarifi, and A. U. Zaman, "A mm-wave wideband slot array antenna based on ridge gap waveguide with 30% bandwidth," *IEEE Transactions on Antennas and Propagation*, vol. 66, no. 2, pp. 1008–1013, 2018.

[40] X. Yang, P. Y. Qin, Y. Liu, Y. Z. Yin, and Y. J. Guo, "Analysis and design of a broadband multifeed tightly coupled patch array antenna," *IEEE Antennas and Wireless Propagation Letters*, vol. 17, no. 2, pp. 217–220, 2018.

[41] T. Goel and A. Patnaik, "Novel broadband antennas for future mobile communications," *IEEE Transactions on Antennas and Propagation*, vol. 66, no. 5, pp. 2299–2308, 2018.

[42] C. A. Balanis, "Antenna theory and applications," in *An Indian Adaptation*, John Wiley & Sons, 4th edition, 2021.

[43] T. Goel and A. Patnaik, "Chapter 14: application based antennas, antenna theory and applications," in *An Indian Adaptation*, C. A. Balanis, Ed., John Wiley & Sons, 4th edition, 2021.

[44] Y. Li and K. M. Luk, "A multibeam end-fire magnetoelectric dipole antenna array for millimeter-wave applications," *IEEE Transactions on Antennas and Propagation*, vol. 64, no. 7, pp. 2894–2904, 2016.

[45] T. Zhang, L. Chen, S. M. Moghaddam, A. U. Zaman, and J. Yang, "Ultra-wideband linearly polarised planar bowtie array antenna with feeding network using dielectric-based inverted microstrip gap waveguide," *IET Microwaves, Antennas & Propagation*, vol. 14, no. 6, pp. 485–490, 2020.

[46] J. Wang, Y. Li, and J. Wang, "Wideband dipole array loaded substrate-integrated horn array with improved sidelobe performance," *IEEE Antennas and Wireless Propagation Letters*, vol. 18, no. 3, pp. 556–560, 2019.

[47] H. He, Y. Chen, and S. Yang, "Novel low profile ultra-wideband capacitance loaded log-periodic monopole array with reduced transverse dimension," *IET Microwaves, Antennas & Propagation*, vol. 13, no. 9, pp. 1443–1449, 2019.

[48] C. Di Paola, S. Zhang, K. Zhao, Z. Ying, T. Bolin, and G. F. Pedersen, "Wideband beam-switchable 28 GHz quasi-Yagi array for mobile devices," *IEEE Transactions on Antennas and Propagation*, vol. 67, no. 11, pp. 6870–6882, 2019.

[49] P. Wang, G. Wen, H. Zhang, and Y. Sun, "A wideband conformal end-fire antenna array mounted on a large conducting cylinder," *IEEE Transactions on Antennas and Propagation*, vol. 61, no. 9, pp. 4857–4861, 2013.

[50] R. Gómez-Villanueva and H. Jardón-Aguilar, "Compact UWB uniplanar four-port MIMO antenna array with rejecting band," *IEEE Antennas and Wireless Propagation Letters*, vol. 18, no. 12, pp. 2543–2547, 2019.

[51] A. Li and K.-M. Luk, "Ultra-wideband endfire long-slot-excited phased array for millimeter-wave applications," *IEEE Transactions on Antennas and Propagation*, vol. 69, no. 6, pp. 3284–3293, 2021.

[52] H. Li, Y. Li, L. Chang, W. Sun, X. Qin, and H. Wang, "A wideband dual-polarized endfire antenna array with overlapped apertures and small clearance for 5G millimeter-wave applications," *IEEE Transactions on Antennas and Propagation*, vol. 69, no. 2, pp. 815–824, 2021.

[53] N. Ojaroudiparchin, M. Shen, and G. F. Pedersen, "Design of Vivaldi antenna array with end-fire beam steering function for 5G mobile terminals," in *2015 23rd Telecommunications Forum Telfor (TELFOR)*, pp. 587–590, Belgrade, Serbia, 2015.

[54] M. M. S. Taheri, A. Abdipour, S. Zhang, and G. F. Pedersen, "Integrated millimeter-wave wideband end-fire 5G beam steerable array and low-frequency 4G LTE antenna in mobile terminals," *IEEE Transactions on Vehicular Technology*, vol. 68, no. 4, pp. 4042–4046, 2019.

[55] R. W. Kindt and B. T. Binder, "Dual-polarized planar-printed ultrawideband antenna array on a triangular grid," *IEEE Transactions on Antennas and Propagation*, vol. 68, no. 8, pp. 6136–6144, 2020.

[56] J. X. Sun, Y. J. Cheng, and Y. Fan, "Planar ultra-wideband and wide-scanning dual-polarized phased array with integrated coupled- marchand balun for high polarization isolation and low cross-polarization," *IEEE Transactions on Antennas and Propagation*, vol. 69, no. 11, pp. 7134–7144, 2021.